Heliyon 9 (2023) e16598

Contents lists available at ScienceDirect

Heliyon

journal homepage: www.cell.com/heliyon

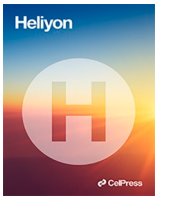

Review article

Nanostructured surface plasmon resonance sensors: Toward narrow linewidths

Kang Yang [a,b,*], Yan Chen [a], Sen Yan [b], Wenxing Yang [a,**]

[a] School of Physics and Optoelectronic Engineering, Yangtze University, Jingzhou, 434023, China
[b] State Key Laboratory of Physical Chemistry of Solid Surfaces, Collaborative Innovation Center of Chemistry for Energy Materials (iChEM), College of Chemistry and Chemical Engineering, Xiamen University, Xiamen, 361005, China

ARTICLE INFO

Keywords:
Plasmonic sensors
Damping
Plasmon linewidth
Structural design
Sensing

ABSTRACT

Surface plasmon resonance sensors have found wide applications in optical sensing field due to their excellent sensitivity to the slight refractive index change of surrounding medium. However, the intrinsically high optical losses in metals make it nontrivial to obtain narrow resonance spectra, which greatly limits the performance of surface plasmon resonance sensors. This review first introduces the influence factors of plasmon linewidths of metallic nanostructures. Then, various approaches to achieve narrow resonance linewidths are summarized, including the fabrication of nanostructured surface plasmon resonance sensors supporting surface lattice resonance/plasmonic Fano resonance or coupling with a photonic cavity, the preparation of surface plasmon resonance sensors with ultra-narrow resonators, as well as strategies such as platform-induced modification, alternating different dielectric layers, and the coupling with whispering-gallery-modes. Lastly, the applications and some existing challenges of surface plasmon resonance sensors are discussed. This review aims to provide guidance for the further development of nanostructured surface plasmon resonance sensors.

1. Introduction

Under the illumination of resonant wavelength, noble metals (such as Au and Ag) can support the coherent oscillations of electrons in metals. These excitations, called as surface plasmon resonances (SPR), can greatly increase the optical extinction cross section of the nanostructure and produce significant near-field enhancement due to the high localization of electromagnetic field beyond the diffraction limit [1–4]. Therefore, noble metal plasmonic nanostructures can be served as SPR sensors by utilizing the high sensitivity of local electromagnetic field to the change of surrounding dielectric environment. In the past decade, benefited from the rapid development of nanofabrication technologies (such as nanosphere lithography and nanoimprint lithography), SPR sensors have found wide applications for the label-free and real-time detection of bio-/chemical species in numerous fields [5–9].

A typical SPR sensing process is shown in Fig. 1, where the resonance spectrum of a SPR sensor shifts to longer wavelength as the refractive index of surrounding environment increases from n to $n+\Delta n$. The sensing performance of various SPR sensors can be evaluated by figure of merit (FOM), which is defined as spectral shift ($\Delta\lambda$) per refractive index unit (RIU) divided by resonance linewidth (full-width at half-maximum, FWHM), namely FOM $= \Delta\lambda/(\Delta n \times$ FWHM). A high FOM has therefore become an important

* Corresponding author. School of Physics and Optoelectronic Engineering, Yangtze University, Jingzhou, 434023, China.
** Corresponding author. School of Physics and Optoelectronic Engineering, Yangtze University, Jingzhou, 434023, China.
E-mail addresses: kangyang@yangtzeu.edu.cn (K. Yang), wenxingyang2@126.com (W. Yang).

https://doi.org/10.1016/j.heliyon.2023.e16598
Received 14 January 2023; Received in revised form 19 May 2023; Accepted 22 May 2023
Available online 24 May 2023

indicator for the excellent sensing performance of a SPR sensor [10,11]. To improve FOM, there are two main directions: 1) enhancing the near-field intensity of SPR sensors to obtain a large spectral shift per refractive index and 2) decreasing the linewidths of SPR sensors. The former can be realized through the fabrication of SPR sensors with strong near-field enhancement [12–15], while the latter requires reducing plasmonic loss of sensor structures [16,17]. For the widely used propagating surface plasmon polaritons (SPP) sensors using prism coupling strategy, it is difficult to realize the flexible tuning of optical properties of the sensor, and the existence of optical components in the device makes it difficult to realize miniaturization and portability, which greatly limits their practical applications [7]. As for localized surface plasmon resonance (LSPR) sensors which are usually based on metallic plasmonic nanoparticles, they do not need to meet momentum matching conditions and the preparation of nanoparticles are relatively simple with low cost [18–20]. The resonant frequency of the sensors can also be flexible tuned by adjusting the material, shape and size of plasmonic nanoparticles. Nevertheless, owing to strong radiative damping of metallic plasmonic nanoparticles, LSPR sensors usually exhibit broad resonance spectra, which greatly limit their sensing performance [10,17].

Recent progresses in micro-/nanofabrications have encouraged the development of metallic plasmonic substrates and numerous nanostructured SPR sensors, such as metallic nanohole [8,21], nanoring [22–24] and nanomushroom arrays [10], have been proposed for sensing applications. Compared with the conventional SPR sensors based on prism coupling configurations and plasmonic nanoparticles, these nanostructured SPR sensors are easy to integrate with imaging and microfluidic systems. In addition, their plasmonic resonances can be excited directly without additional coupling structures, beneficial for the multiplex and high-throughput sensing analysis and the miniaturization and portability of sensing devices. More importantly, various ingenious and flexible structural designs endow the nanostructured SPR sensors with rich optical properties, providing possibilities to enhance near-field intensities and reduce resonance linewidths and therefore improve FOM. Benefited from these characteristics, nanostructured SPR sensors have been widely used for medical diagnosis [25–27], food safety analysis [28–30] and environment monitoring [28,31], etc.

In this review, we aim to introduce effective strategies to improve sensing performance of SPR sensors. We here focus on the current approaches for reducing resonance linewidths instead of the enhancement of near-field intensities. This paper is organized as follows. In section 2, we will introduce the influence factors of plasmon linewidth to facilitate readers of different fields to understand relevant background. In section 3, we focus on the developed strategies for obtaining narrow resonance linewidths. In section 4, the applications of SPR sensors in different fields are reviewed. Lastly, we will discuss in depth the future development of nanostructured SPR sensors.

2. Plasmon linewidth

Plasmon linewidth is associated with the dephasing of the coherent electron oscillation originating from radiative and non-radiative damping [16,32]. Large linewidth can be attributed to a rapid loss of the motion of coherent electron, while narrow linewidth corresponds to a slow dephasing time, namely a long lifetime of surface plasmon oscillation. Generally, the relation between the homogeneous linewidth Γ and the dephasing time T_2 can be expressed as Eq. (1) [17,32],

$$\Gamma = \frac{2\hbar}{T_2} \tag{1}$$

Specifically, the contributions to plasmon dephasing can be written as a sum of several damping terms and plasmon linewidths is therefore described as Eq. (2) [33–35]:

$$\Gamma = \gamma_b + \Gamma_{rad} + \Gamma_{e-surf} + \Gamma_{interface} \tag{2}$$

where γ_b is called bulk damping and is characteristic of material. It originates from electron scattering in metal and can be well described by dielectric function dependent on the incident wavelength [32,33]. The second term Γ_{rad} is radiation damping. It illustrates the energy loss mechanism due to the coupling of plasmon oscillation to radiation field. For plasmonic nanoparticles with large volume

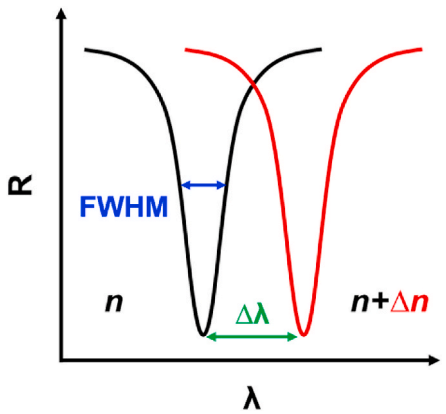

Fig. 1. Illustration of the spectral shift of a SPR sensor as the environmental refractive index changes from n to $n+\Delta n$.

(V), Γ_{rad} can significantly widen plasmon linewidths following its relation with V as $\Gamma_{rad} = 2\hbar\kappa_{rad}V$, where κ_{rad} denotes radiation damping constant varying from 4×10^{-7} to 12×10^{-7} fs^{-1} nm^{-3} [17,36]. The third term Γ_{e-surf} is the damping contribution from electron surface scattering and its influence on plasmon linewidth should be considered when the size of a plasmonic nanostructure is smaller than electron mean free path [32,37]. Usually, the relationship between Γ_{e-surf} and the dimensions of plasmonic nanostructures can be described as $\Gamma_{e-surf} = \frac{S_A V_F}{L_{eff}}$, where S_A, V_F and L_{eff} are the surface scattering constant, Fermi velocity, and effective path length of the electrons, respectively. The last term $\Gamma_{interface}$ is called interface damping. $\Gamma_{interface}$ describes the influence of interface effects originating from the interactions between metals and surrounding medium on spectral linewidths of plasmonic nanostructures [32]. For example, when a plasmonic nanostructure is coated with surface bound molecules, energy or electrons can inevitably transfer from the structure to molecules. It can provide surface plasmons an additional relaxation approach, resulting in a smaller dephasing time and therefore broadening plasmon linewidth [34,35,38].

From the above discussions, it can be seen that the key to obtain narrow plasmon linewidth is to reduce damping [33,39]. As the electron-phonon scattering in non-radiative processes is highly dependent on the temperature, plasmon damping can be therefore reduced by lowering temperature [40]. For example, Liu et al. measured the scattering spectra of single Au bipyramids vs their resonance energies at 77 K (red open circles) and 293 K (blue squares), as illustrated in Fig. 2A [41]. Obviously, the plasmon linewidths measured at 77 K are obviously smaller than their room-temperature counterparts by about 24 meV. And in the work of Xu's group, they investigated the dark-field scattering spectroscopy of a single Au nanowire-Au film nanostructure under different temperature (see Fig. 2B) [42]. It can be seen that the spectral linewidth can be reduced from about 168 to 156 nm when the temperature decreases from 150 to 5 K. Plasmon damping can also be reduced by changing the size of nanostructures. For example, the plasmon bandwidth of spherical Au nanoparticles would be reduced with the decrease of particle size [16]. This phenomenon can be explained by the expression of Γ_{rad} and is regarded as an extrinsic size effect [16]. In addition to reducing damping, there are also attempts to narrow linewidths from the point of loss compensation [43,44]. For example, Luca and coworkers investigated the absorbance spectra of a nanoparticle composed of Au core and silica shell without and with a gain material adding into the shell [45]. The gain medium can partially compensate the intrinsic losses of metal material and lead to a small decay rate, therefore the particle with gain shows a narrower linewidth than the counterpart without gain.

Although these strategies mentioned above can show partial effects on decreasing FWHM, the achievement of desired narrow linewidths (down to a dozen or even a few nanometers) is still difficult, which severely limits the performance in SPR sensing. Therefore, the pursuit of more powerful methods for reducing plasmon linewidths has attracted wide attentions.

3. Solutions for achieving narrow linewidths

The vast development on micro-/nanofabrication techniques has made it possible to obtain arbitrary structural morphologies and configurations. Therefore, the optical performance of plasmonic nanostructures, such as the peak position and intensity of resonance spectra, and the linewidths of interest in this review, can be designed and tailored in a targeted manner. In this section, we will systematically introduce various approaches for obtaining narrow plasmon linewidths.

3.1. *Constructing plasmonic nanostructures that support surface lattice resonance (SLR)*

SLR, also called collective resonances, is an optical phenomenon due to the coupling between LSPR and diffractive modes [46,47]. If plasmonic nanoparticles are organized in an ordered way, they can scatter incident light and thus result in diffraction. When one of the diffracted light is coupled to the localized plasmon resonances of individual nanoparticle, SLR can occur and greatly suppress the radiative damping of the plasmonic nanostructure, resulting in an ultra-narrow spectral linewidth that even reaches 1–2 nm. Benefited from the excellent characteristics, SLR has attracted wide attentions in the field of SPR sensing [48,49].

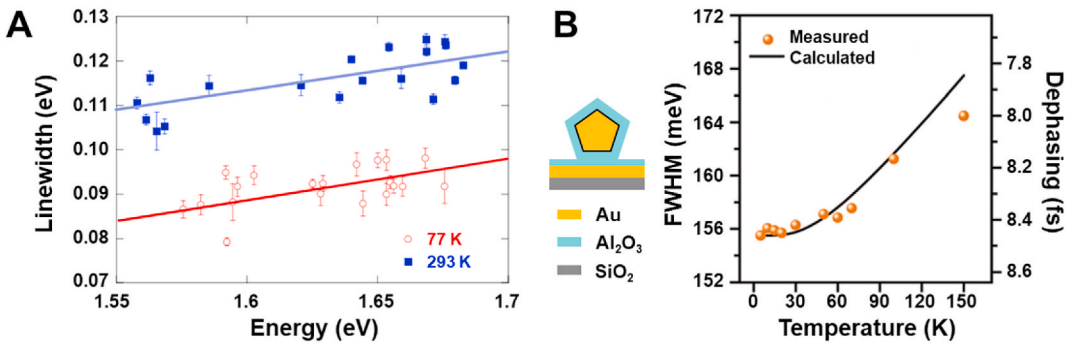

Fig. 2. A) Plasmon linewidths of scattering spectra of single Au bipyramids as a function of resonance energy (linearly fitted) when the temperature is 293 K (blue) and 77 K (red). Reproduced with permission [41]. Copyright 2009, American Physical Society. B) Plasmon linewidths (orange dots) and dephasing time (solid black line) of the Au nanowire-Au film nanostructure under a temperature ranging from 0 to 150 K. The inset displays the structural diagram consisting of a Au-nanowire over a Au mirror. Reproduced with permission [42]. Copyright 2020, De Gruyter.

The theoretical elucidation of SLR phenomenon can be achieved by utilizing coupled dipole approximation [46,50]. In the method, each nanoparticle is treated as a dipole and thus an array composed of N nanoparticles can be regarded as an array of electric dipoles. In an infinite array, the effective polarizability (α_{eff}) of different nanoparticle is considered to be the same and can be expressed through Eq. (3) [46,47],

$$\alpha_{eff} = \frac{1}{\left(\frac{1}{\alpha_s} - S\right)} \tag{3}$$

and the corresponding extinction cross-section (C_{ext}) can be described as Eq. (4):

$$C_{ext} = 4\pi k \mathrm{Im}\left(\alpha_{eff}\right) \tag{4}$$

where α_s is polarizability of an isolated plasmonic nanoparticle, S is retarded dipoles sum originating from other nanoparticles, and k denotes the wavenumber of incident light. It is clear that when S equals to $\frac{1}{\alpha_s}$, C_{ext} achieves infinite, indicating that SLR mode occurs.

SLR can be achieved in various plasmonic nanostructures, including one dimensional (1D) chains, 2D arrays and 3D substrates through the elaborate adjustment of size, morphology and arrangement of nanoparticles and the period of nanoarrays [46]. For example, by using dipole sum approach, Zou et al. investigated the extinction spectra (Fig. 3A) of a 1D chain and a 2D hexagonal array composed of Ag NPs with diameter of 100 nm [51]. As the separation distance between nanoparticles increased, they found the resonance spectra of the two structures both narrowed significantly and shifted to longer wavelength. Specifically, the calculated linewidth of chain can reach 3.7 nm and even 1.5 nm when the period is 470 nm and 500 nm, respectively, much smaller than that of single Ag nanoparticle (dotted line in Fig. 3A–i). However, the resonance intensity decreased dramatically when the chain period increased. The similar phenomena can also be observed for the 2D array when the nanoparticle spacing distance increased, albeit with linewidths that are slight larger (Fig. 3A–ii). Experimentally, Offermans et al. fabricated several Au square arrays on quartz substrate (Fig. 3B–i) by utilizing e-beam lithography and ion-milling [52]. It is clear that as the lattice constants increased from 300 to 600 nm, transmittance spectrum of the Au array narrowed considerably and the resonance peak shifted toward lower frequency simultaneously (Fig. 3B–ii). These phenomena can be explained by the more negative retarded dipole sum of the array as the lattice constant increased, leading to the partial cancellation of damping and therefore a smaller resonance linewidth. In addition to the lattice constant, the size of plasmonic nanoparticle also shows significant influence on the position and width of resonance spectra. As shown in Fig. 3B–iii, the

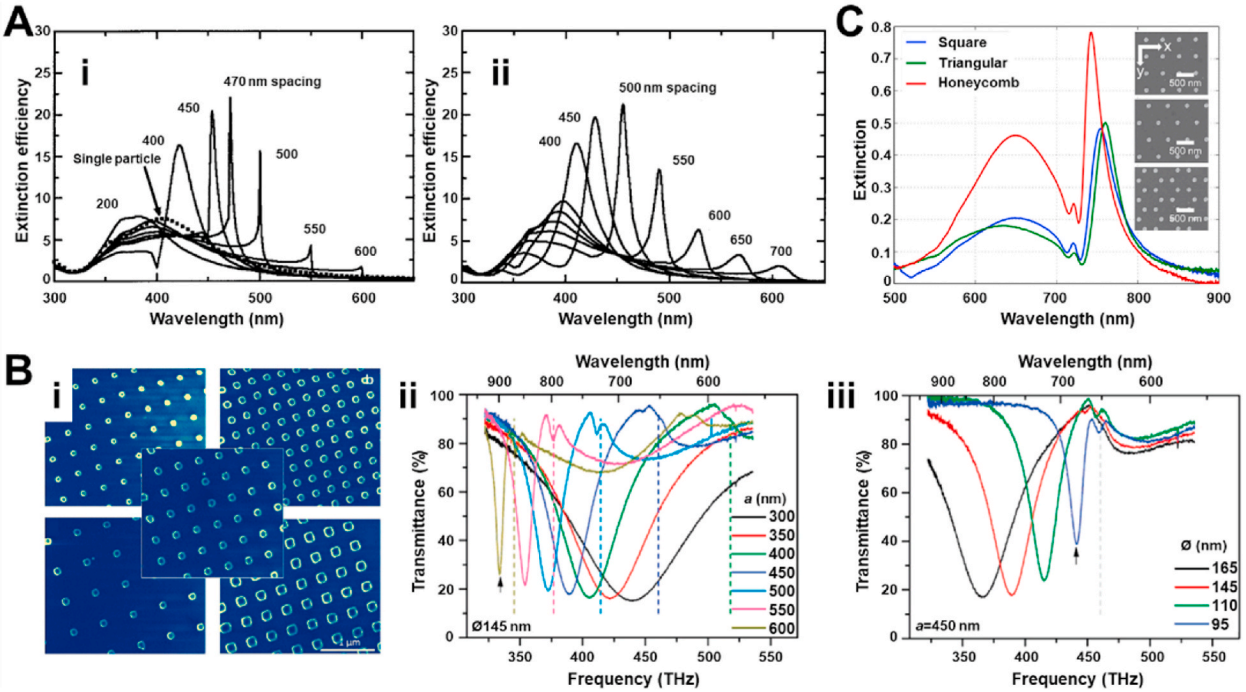

Fig. 3. A) Calculated extinction spectra of (i) a 1D AgNPs chain and (ii) a 2D hexagonal AgNPs array over different spacing distances. Reproduced with permission [51]. Copyright 2004, American Institute of Physics. B) (i) SEM images of AuNPs arrays with different diameters and lattice constants. (ii,iii) Transmittance spectra of the AuNPs arrays under different lattice constants (a) and particle diameters (d). Reproduced with permission [52]. Copyright 2011, American Chemical Society. C) Measured extinction spectra of AgNPs arrays with different arrangements. The insets show the SEM images of a square array (top), a triangular array (middle) and a honeycomb array (bottom). Reproduced with permission [53]. Copyright 2014, American Physical Society.

resonance spectra of the Au square array shifted to longer frequency and narrowed significantly with the decrease of the nanoparticle diameter from 165 nm to 95 nm. Finally, by optimizing the two parameters, SLR in the Au square array can offer an improvement in sensing performance by more than one order of magnitude than that of localized plasmon resonance of disordered Au nanoparticle arrays. In addition to structural parameters, the influence of nanoparticles arrangement in plasmonic arrays on SLR is also investigated. As shown in Fig. 3C, Humphrey and Barnes fabricated square, triangular and honeycomb arrays composed of Ag nanoparticles by using electron-beam lithography [53]. They found that the differences in spectral linewidths of these arrays are very small, demonstrating SLR can be generated in various plasmonic arrays with no one configuration showing a distinct advantage in terms of resonance linewidth.

3.2. *Constructing plasmonic nanostructures that support plasmonic Fano resonance*

Fano resonance originates from spectral interference between a discrete state and a broad continuum resonance [54–56]. Different

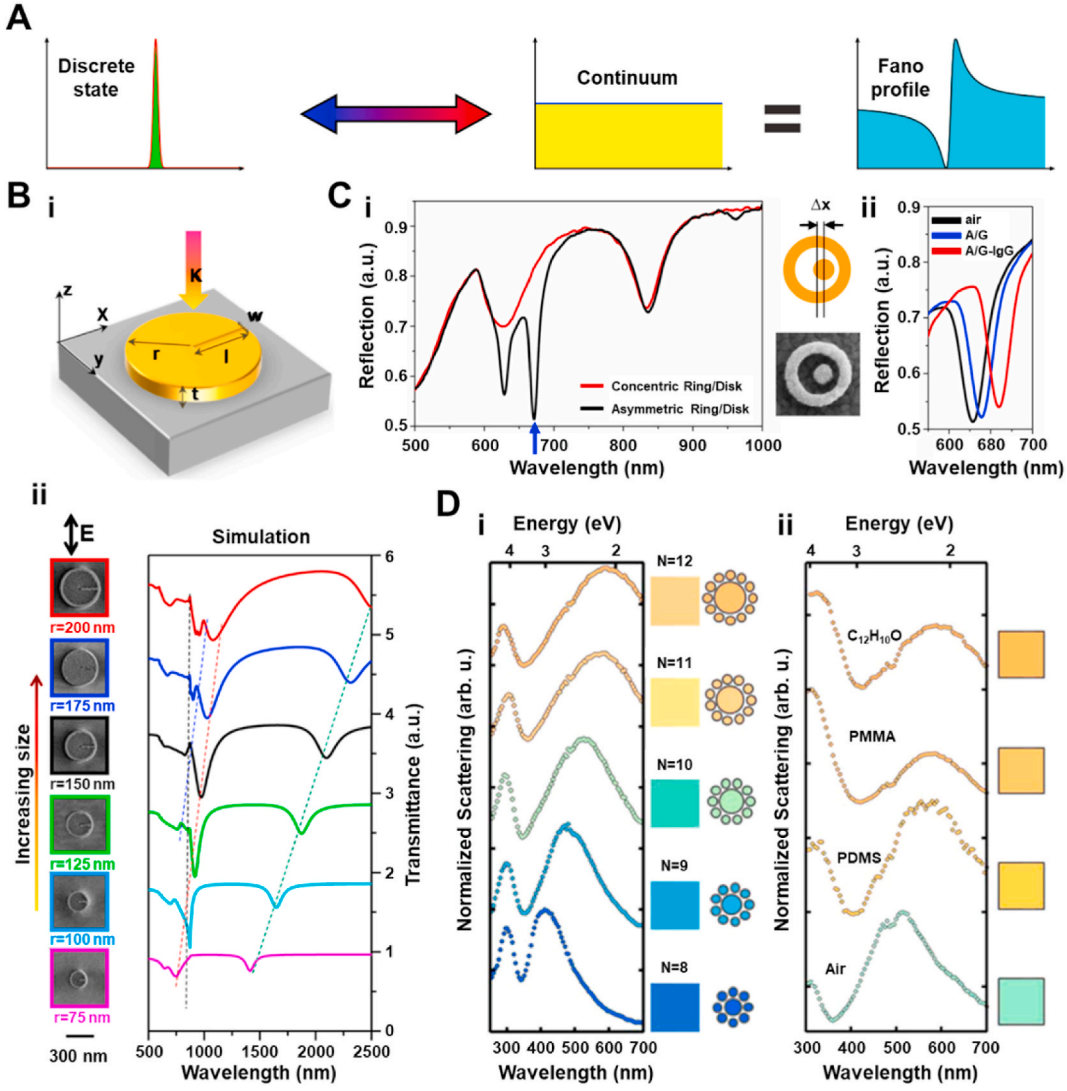

Fig. 4. A) Diagram view of Fano resonance as a superposition of a discrete state with a continuum. Reproduced with permission [57]. Copyright 2010, American Physical Society. B) (i) 3D schematic of a single Au split nanodisk. (ii) SEM images (left) and calculated transmittance spectra (right) of the fabricated split nanodisks under different radius from 75 nm to 200 nm. Reproduced with permission [60]. Copyright 2016, American Chemical Society. C) (i) Reflection spectra of concentric (red) and asymmetric ring/disk cavities (black) with $\Delta x = 30$ nm. (ii) The spectral change of the asymmetric ring/disk cavities after the introduction of protein A/G (blue) and IgG antibody (red). Reproduced with permission [66]. Copyright 2012, American Chemical Society. D) (i) Normalized scattering of a Al nanocluster with different satellite particle number (N). (ii) Experimental spectra of a nanocluster ($N = 10$) placed in different environments. The colorimetric phenomena are shown in the right of each plot. Reproduced with permission [69]. Copyright 2015, American Chemical Society.

from a Lorentzian lineshape, Fano resonance shows a distinctly asymmetric spectrum (illustrated in Fig. 4A), which can be described by famous Fano formula as Eq. (5) [56,57],

$$\sigma(E) = D^2 \frac{(q+\Omega)^2}{1+\Omega^2} \tag{5}$$

where E is the energy, $D^2 = 4\sin^2\delta$ (δ denotes the continuum phase shift), $q = \cot\delta$ denotes the parameter determining asymmetry degree. $\Omega = \frac{2(E-E_0)}{\Gamma}$, where Γ and E_0 are the resonance width and energy, respectively.

Plasmonic Fano resonance with narrow resonance linewidth and high spectral contrast have been obtained in various plasmonic nanostructures through ingenious structural designs [54,58,59]. Plasmonic Fano resonance can be first generated in a single disk nanostructure [60–63]. For example, Zhang et al. fabricated a single plasmonic split nanodisk (shown in Fig. 4B–i) with an extremely narrow split gap down to 15 nm [60]. The structure can support pronounced Fano resonance due to the mode interference between the bright antibonding dipole mode of the split disk and the subradiant mode supported by the narrowsplit gap. Fig. 4B–ii shows the transmittance spectra of the split nanodisk with different sizes, where the split length of structures equals to their respective radius. It can be seen that as the radius varies from 75 nm to 200 nm, the spectra exhibit significant change and the linewidth (red dashed line) increases simultaneously, indicating the stronger radiative loss when the structure becomes larger. Alternatively, plasmonic Fano resonance is also supported by heterogeneous dimer disk nanostructures [64–66]. As shown in Fig. 4C, Cetin and Altug used electron-beam lithography and fabricated an asymmetric ring/disk structure on a Au layer [66]. The structural asymmetry degree is determined by the shift amount (Δx) of the disk from the center of the concentric system along the polarization direction (see the right part in Fig. 4C–i). Compared with the concentric ring/disk structure, it is clear that the asymmetric ring/disk structure exhibited distinctly different spectral characteristics with a narrow resonance linewidth as small as 9 nm (indicated by a blue arrow in Fig. 4C–i). By using the asymmetric nanostructure, they experimentally achieved a high FOM value of 72 for reliable detection of monolayer/bilayer proteins. Furthermore, plasmonic Fano resonance can also be observed in clusters of plasmonic nanoparticles [67,68]. In Fig. 4D, Halas et al. fabricated a Al nanocluster consisting of a core disk surrounded by N satellite disks (N is the number of the satellites) [69]. By adjusting the satellite nanoparticle size and number, the spectrum of the nanocluster can be tuned from the near-UV into the visible region (Fig. 4D–i). The characteristic enables the structure for plasmonic colorimetric sensing, where the presence of analytes can be detected directly from observable color changes without the need of photodetectors and spectral analyzers (Fig. 4D–ii). However, the linewidth of the cluster structure is a little broad, which limits the sensing performance. In addition to the mentioned configurations, many other structures supporting Fano resonance have also been proposed recently. Kazanskiy et al. developed a side-coupled circular cavity (SCCC) and a ring encapsulated circular cavity (RECC) [70]. Due to the strong coupling of electromagnetic waves in the cavity, the RECC configuration offers a Fano resonance, which results in a higher FOM (691/RIU) than the one offered by

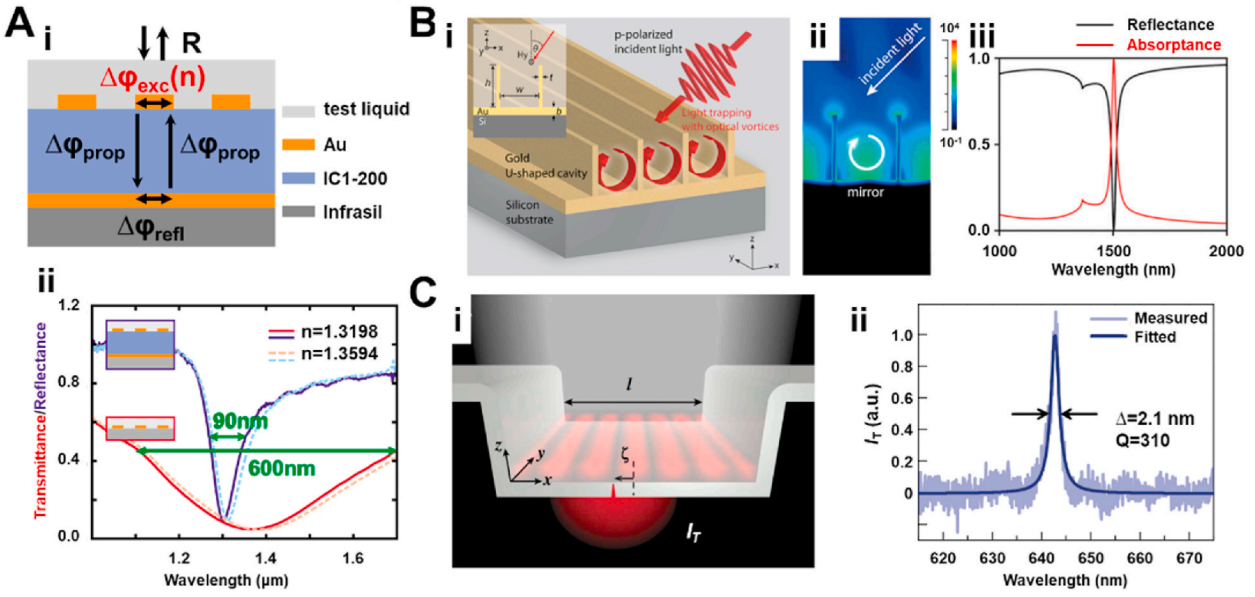

Fig. 5. A) (i) The phase shifts occurring at one roundtrip of an electromagnetic wave in the Au nanorod-microcavity structure. (ii) Comparison of the experimental spectra for Au nanorods alone and Au nanorods combined with a cavity. Two environments (n = 1.3198 and 1.3594) are used. Reproduced with permission [74]. Copyright 2010, American Institute of Physics. B) (i) Diagram view of the U-cavity structure. (ii) Simulated electric field density distributions of the coupling of the ridge mode to the hollow U-cavity. (iii) Simulated reflection and absorption spectra of the U-cavity structure. Reproduced with permission [77]. Copyright 2014, Wiley-VCH. C) (i) Illustration of the trench plasmonic resonator. (ii) Transmitted light outcoupled by the slit aperture under the illumination of an open side of the cavity with incoherent white light. Reproduced with permission [76]. Copyright 2017, American Association for the Advancement of Science.

SCCC (18.74/RIU) in biosensing application.

3.3. Constructing plasmonic nanostructures coupled with photonic cavities

The broad resonance spectrum of a plasmonic nanostructure can also be narrowed by coupling with a photonic cavity [71–73]. Generally, the radiative loss of the formed photonic-plasmonic system can be greatly reduced when Eq. (6) is fulfilled [74,75],

$$\Delta\varphi_{tot} = 2\Delta\varphi_{prop} + \Delta\varphi_{refl} + \Delta\varphi_{exc} = 2\pi N \tag{6}$$

where $\Delta\varphi_{tot}$ is the total phase shift of light accumulated during one roundtrip in the cavity, $\Delta\varphi_{prop}$ is the phase shift resulting from the light propagation through the cavity and is closely related to the thickness of the cavity, $\Delta\varphi_{refl}$ denotes the phase shifts upon reflection at the cavity mirror and can be obtained through Fresnel equations, $\Delta\varphi_{exc}$ originates from the resonance mode of the plasmonic nanostructure, and N is an integer. It is clear that the linewidth of the coupled system can be flexibly tuned by simply adjusting the cavity thickness.

Experimentally, Giessen' group placed the Au nanorods array at Bragg distance above a Au mirror, as shown in Fig. 5A–i [74]. The refractive index and thickness of the dielectric cavity are 1.4 and 380 nm, respectively. Through the structural design, they can decrease the resonance linewidth of the substrate from 600 nm to 90 nm (Fig. 5A–ii) and increase the FOM value by a factor of 3.1, allowing for a much more sensitive detection of the change of surrounding environment. In addition to vertical direction, the cavity system can also be achieved in horizontal direction [76,77]. For example, Delaunay et al. proposed a Au U-cavity structure composed of Au nanofins on a Au film, as shown in Fig. 5B–i [77]. Ridge mode coupled U-cavity with mirrored surface plasmons supports an intense optical vortex, leading to a full light trapping (Fig. 5B–ii). Therefore, a linewidth of 14 nm (Fig. 5B–iii) can be experimentally observed in the far field spectra with a sensing sensitivity as high as 791 nm/RIU. Similarly, Zhu et al. designed a trench plasmonic nanostructure consisting of an opaque Ag film forming two vertical Ag sidewalls and a horizontal floor (Fig. 5C–i) [76]. Under the illumination of white light, SPP can be launched and propagate across the cavity and reflect efficiently by the sidewalls. A sub-wavelength slit parallel to the sidewalls is fabricated in the cavity floor, allowing for efficient coupling between the SPP field in cavity and the fundamental propagating mode of the slit. Finally, the structure can produce a Lorentzian lineshape with a narrow FWHM of 2.1 nm and a high quality factor of about 310 (Fig. 5C–ii).

3.4. Constructing plasmonic nanostructures inherent with ultra-small resonators

Although the methods in above sections have been widely adopted to obtain narrow linewidths, the challenge is that they require

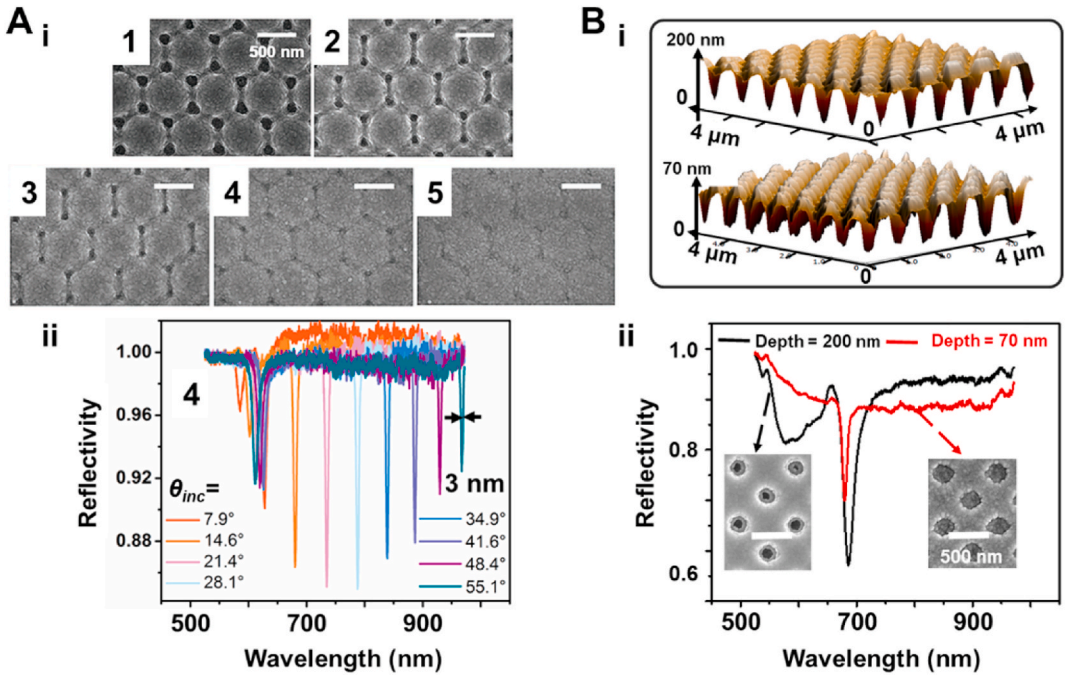

Fig. 6. A) (i) SEM images of five hexagonal arrays with nanoholes and nanoslits of different depths. (ii) Reflectance spectra of array 4 under different incident angles (θ). Plasmon linewidth down to 3 nm can be obtained at incident angle (θ) of 55.1°. Reproduced with permission [11]. Copyright 2018, Wiley-VCH. B) (i) AFM images and (ii) resonance spectra of Au orthorhombic nanohole arrays with a shallow hole depth (right) and a deep hole depth (left). Reproduced with permission [7]. Copyright 2021, Wiley-VCH.

elaborate structure designs to achieve effective couplings of different optical modes. Alternatively, resonance linewidth can be reduced by minimizing the size of resonators of plasmonic nanostructures to prolong the lifetime of resonance modes, therefore narrow spectral peaks can be achieved according to Eq. (1) mentioned in section 2.

In the work of Ren's group, they fabricated a series of Au hexagonal arrays under the assistance of a tunable holographic lithography method, as shown in Fig. 6A–i [11]. By minimizing the feature sizes of nanoholes and nanoslits of these array structures, they can achieve a narrow linewidth smaller than 8 nm over a wide optical range from 600 nm to 960 nm and a minimum linewidth down to 3 nm at 960 nm (Fig. 6A–ii). Benefited from the ultra-narrow and almost perfect Lorentzian lineshape of the resonance spectrum, a high sensitivity of 5833 nm/RIU and FOM value of 730 can be achieved. In addition to the hexagonal array, plasmonic nanostructures with other morphologies can also produce narrow resonance spectra through this strategy (namely reducing the feature sizes of resonators). As illustrated in Fig. 6B–i, Ren et al. recently fabricated two Au orthorhombic arrays with different hole depths [7]. It is clear that the plasmon linewidth of the array with shallow depth is much smaller than that of the deep one (Fig. 6B–ii), demonstrating the universality of the method for obtaining narrow resonance spectra.

3.5. Other methods to obtain narrow linewidths

In addition to the abovementioned methods, there are also many other approaches for achieving narrow resonance spectra. In this section, a brief introduction of these strategies is provided.

Platform-induced modification: Usually, metallic SPR sensors need to be fabricated on supporting platforms, therefore the interaction between metal nanostructures and platforms may greatly influence the resonance spectra, providing the possibility for reducing linewidths [78,79]. As illustrated in Fig. 7A–i and ii, Halas's group observed that the dipolar plasmon resonance linewidth of a Al nanoparticle narrows remarkably when it coupled to an underlying Al film [80]. The phenomena are generated due to the reduction in radiative loss originating from the Al film-mediated hybridization of the dipolar and quadrupolar plasmons of Al nanoparticle. Similarly, by replacing a silica platform with a Au film (Fig. 7A–iii), Lei et al. realized pronounced linewidth shrinking (Fig. 7A–iv) in a Au nanosphere dimer [81]. Using this structure, they achieved a photoluminescence intensity enhancement up to nearly 200 times with a much narrower emission linewidth than the silica-supported dimer.

Alternating different dielectric layers: In 2007, Kaliteevski et al. theoretically discovered a plasmon-polariton state called as Tamm plasmon-polaritons (TPPs) in the nanostructure formed between a metal and a dielectric distributed Bragg reflector [82]. The Bragg mirror consists of alternating dielectric layers of different refractive indices. Through the design, a photonic bandgap can be formed and hence achieve the confinement of TPPs in the structure. Due to the low dissipation losses of dielectric layers, TPPs can produce a narrow and intense spectral feature [83–85]. For example, Kumari et al. investigated the reflectance property of the Tamm plasmon system consisting of a layer of Au film and periodic multilayers of TiO_2 and SiO_2 [86]. The structure exhibits a distinctive

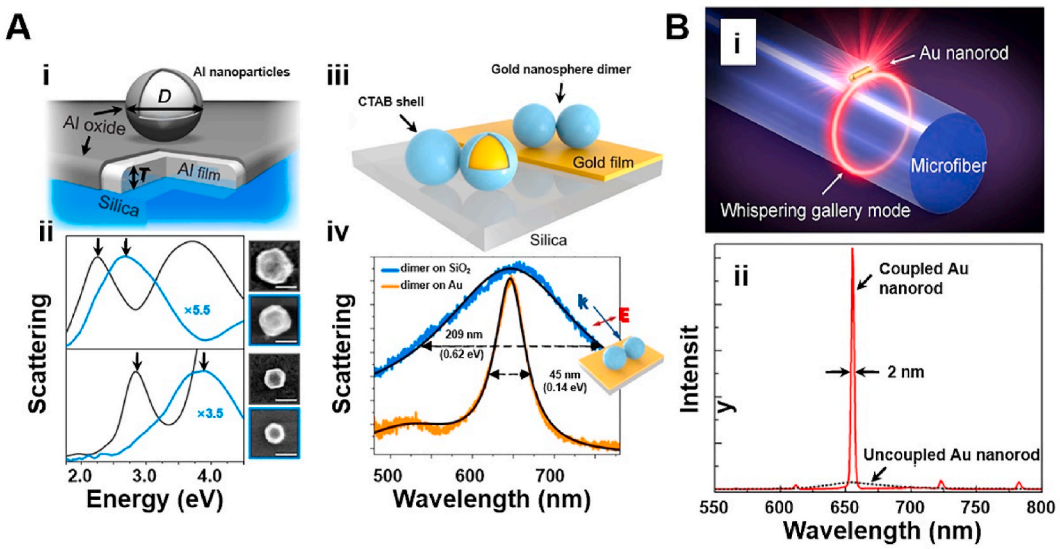

Fig. 7. A) (i) Schematic of a Al nanoparticle positioned on a Al film and (ii) the measured dark-field scattering spectra of a 180 nm Al nanoparticle (top) and a 100 nm Al nanoparticle (bottom) when placed on a Al film of thickness $T = 35$ nm (gray) or directly placed on a silica substrate (blue). Scale bar: 100 nm. (iii) Diagram of two cetyltrimethylammonium bromide-coated (blue) Au nanosphere dimers placed respectively on a thin Au film (yellow) and on a glass substrate (gray). (iv) Scattering spectra of the Au dimers on the Au film (orange) and on silica (blue). (i,ii) Reproduced with permission [80]. Copyright 2015, American Chemical Society (iii,iv) Reproduced with permission [81]. Copyright 2017, American Chemical Society. B) Coupling a Au nanorod with the whispering gallery cavity of a silica microfiber for a dramatic reduction in plasmon linewidth. (i) Schematic of the hybrid structure. (ii) Scattering spectra of single Au nanorod coupled to a silica microfiber with a diameter of 1.46 μm (red solid line) or directly placed on a glass slide (black dotted line). Reproduced with permission [93]. Copyright 2015, American Chemical Society.

narrow spectral feature at 658 nm when Au thickness is 60 nm and the number of unit cells of Bragg mirror is 10.

Coupling with whispering-gallery-mode: Through total internal reflection, whispering-gallery-mode (WGM) can confine light energy effectively and achieve resonances with high quality [87–89]. Therefore, the combination of plasmonic nanostructures with WGM can compensate the intrinsic damping loss of metal materials, providing possibilities for the reduction of plasmon linewidths [90–92]. In the work of Tong's group, they reported a significant narrowing in resonance linewidth of a single Au nanorod through coupling with a WGM of a silica microfiber [93]. Fig. 7B–i shows the schematic diagram of the hybrid structure. Compared with the broad resonance spectrum of a Au nanorod placed on a glass slide, the Au nanorod in the coupling system shows an extremely narrow plasmon linewidth down to 2 nm with a significant enhancement in the scattering peak intensity (Fig. 7B–ii).

4. Applications of SPR sensors

Benefited from the significantly enhanced near-field under resonance wavelength, SPR nanostructures can effectively covert the variation in refractive index of surrounding medium into the change of resonance spectra (such as the shift of peak position). Therefore, SPR sensors have found wide applications in numerous fields [94–99]. In this section, the applications of SPR sensors in medical diagnostics, food safety analysis and environmental monitoring are briefly introduced.

4.1. Medical diagnostics

SPR sensors have attracted wide attentions in the field of medical diagnosis for rapid and sensitive detection of various targets, such as cancer markers, allergy markers and drugs [25,26,100–105]. For example, microRNAs (miRs), as a typical analyte, can modulate numerous biological processes by targeting with specific mRNA moieties for translational repression or degradation. Therefore, the level of miRs in plasma and other biological fluids can serve as diagnostic and prognostic disease biomarkers [106–108]. In the work of Sardar's group, they described a direct hybridization approach for the detection of miR-X (X = 21 and 10b) in human plasma of pancreatic cancer patients [107]. The sensor substrate is composed of Au nanoprisms attached onto a glass substrate. The sensing mechanism is to change the local environment around the sensor through the hybridization between complementary single-strand DNA (ssDNA) pre-modified on the surface of nanoprisms and the target miR-X, thus the resonance peak can shift to a longer wavelength. Finally, they achieved the sensitive detection of miR-21 with a limit of detection (LOD) of 23–25 fM and miR-10b with a LOD of 50 fM. In another example, Altug et al. fabricated a Au nanohole array for the real-time analysis of vascular endothelial growth factor (VEGF) secretion [109], which plays a key role at various stages of cancer development, such as angiogenesis, progression and metastasis. The sensor surface was first modified with PEGylated alkanethiol to covalently bond with streptavidin. Then the biotinylated anti-VEGF was immobilized by the robust streptavidin-biotin interaction for capturing VEGF secreted by cancer cells. By monitoring the change of the extraordinary optical transmission (EOT) spectrum before and after binding, the sensor shows an outstanding sensitivity of 145 pg/mL (5.37 pM) for VEGF detection. Recently, SPR sensors were also widely used for the detection of severe acute respiratory syndrome coronavirus 2 (SARS-CoV-2) variants, which caused the global pandemic of coronavirus disease 2019 (COVID-19) [110,111]. For example, in the work of Kim' group, they developed a bioresponsive nanogel-based SPR platform for the rapid detection of SARS-CoV-2 in buffers and human blood [110]. Compared with other commercial methods, the proposed strategy shows a better selectivity and sensitivity.

4.2. Food safety analysis

The increasing attention to food safety has driven considerable development of SPR sensing for food quality analysis. Many analytes, such as pathogens, toxins and allergens, have be targeted by SPR sensors [28,30,112–114]. For example, in the work of Yu's group, they proposed a dielectrophoresis (DEP)-SPR sensor for the sensitive detection of *Escherichia coli* [115]. The dually functional DEP-active interdigitated electrodes were used to sustain strong SPR and simultaneously increase the mass transport of bacterial cell to the sensing surface through DEP. Through proper chemical modification, the sensor device provides a LOD of 3.0×10^2 CFU/mL in the detection of *E. coli*, nearly 5 orders of magnitude higher than that of traditional SPR chip. In addition to the single species analysis, SPR sensors can also be used for multiplex detection [116,117]. For example, Tabrizian's group introduced a SPR microarray for the analysis of 16S rRNA analytes from three pathogenic species simultaneously: *Legionella pneumophila, Pseudomonas aeruginosa, and Salmonella typhimurium* [116]. During the sensing process, the 16S rRNA to be measured was first modified on the sensor by surface-bound DNA probes. Then, the Au nanoparticles-grafted DNA probes were introduced and hybridized with the desired region of 16S rRNA, forming the sandwich assemblies of long DNA−RNA and hence increasing SPR signals. The developed system shows a high selectivity for the sequences analysis of 16S rRNA in total RNA mixed samples extracted from the three pathogenic strains with a LOD of 10 pg/mL and a large detection range of 0.01–100 ng/mL.

4.3. Environmental monitoring

Due to the significant development of industry, SPR sensors have also served as important platforms for the monitoring of various environmental pollutants, such as toxic/dangerous gases and heavy metals [31,118–122]. For example, Zaghloul et al. fabricated a Cu-benzenetricarboxylate (Cu-BTC) metal organic frameworks (MOF)-coated Au nanohole array for the analysis of acetone and ethanol vapors [123]. The 3D framework of Cu-BTC consists of pores of different sizes and shapes, facilitating the adsorption of gas molecules. Thus, the peak intensity of the nanohole array can be changed due to the increased refractive index of local environment. In

this way, the sensor can response to 500 nmol/mol (ppb) of acetone or ethanol vapors under room temperature. In addition to flexible external modifications, the inherent properties of materials used in sensors can also be utilized to achieve the analysis of targets [118,120,124]. For example, in the work of Jin's group, they fabricated a palladium nanogroove array for hydrogen sensing because palladium can absorb hydrogen and undergo a lattice expansion with a phase transition from a metal to a metal hybride [124]. On the one hand, each palladium groove on an elastic substrate can act as a mechanically reconfigurable plasmonic cavity. On the other hand, the presence of the flexible substrate can not only amplify the change of SPR signal but also improve the reliability and life of the sensor. Finally, they can realize the sensitive detection of hydrogen with an LOD (in N_2) of 0.1% and a sensing resolution of 0.013%. In addition, a quick response time (on a time scale of seconds), an excellent recyclability (>10 cycles), and a long-term stability (90% of original spectral shift after 24 days) can also be achieved simultaneously, demonstrating the great potential of the hydrogen sensor for practical applications.

In addition to the examples mentioned above, SPR sensors can also serve as an ideal tool for sensitive detection of many other targets [28,31,125]. Table 1 shows some typical applications of SPR sensors [100,126–129]. The interested readers are suggested to refer to other articles on this topic for more details.

5. Summary and outlook

In the past few decades, nanostructured SPR sensors have obtain significant development due to the great progresses in theoretical researches and fabrication technologies. Various sensor structures with excellent performance have been proposed and manufactured to meet the needs in different application fields. In this review, we have introduced the influence factors of plasmon linewidths and the effective strategies to obtain narrow FWHM, as well as several practical applications of nanostructured SPR sensors. In addition to the contents discussed here, there are also several important issues remaining for the development of SPR sensor structures in the future.

Machine learning-assisted structural design for higher fabrication efficiency. Generally, the design of a nanostructured SPR sensor is usually hindered by a convoluted and iterative process, involving tedious modeling, fabrication and characterization [130–132]. It is challenging and time-consuming, which seriously limits the preparations and applications of SPR sensors. In recent years, the rapid development of machine learning has redefined the way for the processing of large data sets and enabled structural inferences from systems that are difficult to model. Therefore, machine learning shows great potential for structural designs of plasmonic substrates [133–137]. For example, Muskens et al. proposed an approach that combines the coupled dipole approximation with deep artificial neural networks for accelerate universal electrodynamical simulations of 3D nanostructures by many orders of magnitude [138]. This work provides a generalized accurate prediction for near-/far-fields of arbitrary 3D plasmonic and dielectric nanostructures with a small error in the order of around five percent. Indeed, there is still numerous works can be done in this direction to obtain nanostructured SPR sensors with extremely narrow linewidths and excellent sensitivity [139,140].

Low loss structural system for better sensing performance. Despite the low loss of widely used noble metals (such as Au and Ag), the optical properties of plasmonic nanostructures are still fundamentally limited by the intrinsic damping of the metallic resonator elements. Therefore, there is a persistent pursuit of low-loss materials for the construction of plasmonic nanostructures [141–143]. Recently, Zhu et al. took advantage of the low melting point of sodium and developed a thermal-assisted spin-coating method for the fabrication of stable sodium-based plasmonic nanostructures [144]. After systematical comparison, the structure shows better plasmonic performance than the noble-metal based counterpart primarily because of the ultralow interband damping rate of alkali metals. In addition, the recent development of hybrid plasmonic-dielectric nanostructures has attracted wide attentions and many interesting phenomena, such as strong coupling and bound states in the continuums (BICs) [145–150], have been observed in these structures, providing possibilities for the performance improvement of nanostructured SPR sensors. For example, Görrn et al. fabricated a large scale hybrid waveguide consisting of a flat Ag film embedded in a dielectric core with dielectric cladding [151]. They provided the experimental evidence for the existence of hybrid BICs and theoretically demonstrated that the sensor can achieve a FOM as high as 1.43×10^5/RIU, nearly one order of magnitude higher than that of dielectric BICs despite of the introduction of a lossy metal. These works demonstrate that there is a plenty of room for improving the performance of nanostructured SPR sensors unattainable by using conventional noble metals.

High-throughput, portable sensing system for practical applications. High-throughput and multi-channel detection is an important topic for the application of SPR sensors because it involves not only the fast detection of large number of samples but also the

Table 1
Typical applications of SPR sensors.

Device	Material	Sensing application	Characteristics	References
periodic nanohole array	Au	exosomes	high throughput for massively parallel detection	[100]
periodic nanohole array	Au	extracellular vesicles	multiplexed profiling	[126]
nanoparticle	Au, Pd, Cu	hydrogen	good long-term stability	[127]
nanoparticle	Au	Anti-receptor binding domain antibodies	revealing both the amount and binding kinetic profiles information, short time-to- result	[128]
nanoparticle	Ag, Fe_3O_4	Leukocyte cell-derived chemotaxin 2	excellent binding efficiency, high sensitivity	[129]

accuracy and reliability of the results through mutual verification. Recently, the vast development of integrated microfluidic SPR chip with multiple-channel has spurred a series of progresses toward this direction [152–154]. For example, Yavas et al. presented a SPR sensor platform integrated with state-of-the-art microfluidics for simultaneously self-calibrating, automated and multiplexed real-time detection of four breast cancer protein markers in human serum [155]. Similarly, Sugai et al. proposed a multichannel microfluidic SPR sensing system for damage-free characterization of cells by pattern recognition [156]. In addition to ensuring the speed and accuracy of detection process, the integration of SPR sensors into portable devices is another key to the technology in daily applications [157–159]. Actually, great efforts are being made to achieve the solution [160,161]. For example, Liu et al. developed a portable fiber-optic SPR biosensor using a smart phone as a sensing platform [162]. The fiber-optic SPR structure as a sensing element can greatly enhance the simplicity and flexibility of the optical alignment and light coupling. The smart phone is used as the light source and detector. The proposed cost-effective and portable SPR sensor platform shows great potential for applications in the fields such as point-of-care tests, ubiquitous healthcare and environmental monitoring. These works indicate that more relevant efforts are necessary for the further practical applications of nanostructured SPR sensors.

Last, nanostructured SPR sensors with chiral plasmonic configurations have also attracted wide attentions in bio-/chemical sensing fields [163–166]. Usually, the circular dichroism response of chiral SPR sensors to the change of surrounding environment is superior than that measured from conventional measure methods (extinction, scattering and reflectance spectroscopies) [167–169]. It means that the sensing performance of SPR sensors may be greatly improved through flexible structural design and appropriate measurement tools.

Overall, the on-going emergence of new structural designs, processing and characterization techniques can continually boost the development of nanostructured SPR sensors and thus meet the new demands in different applications. We expect the SPR sensing technology to play an increasingly significant role in various interdisciplinary fields in the future.

Author contribution statement

All authors listed have significantly contributed to the development and the writing of this article.

Funding statement

This work was sponsored by the National Natural Science Foundation of China (22202017, 11774054 and 12075036).

Data availability statement

No data was used for the research described in the article.

Declaration of competing interest

The authors declare that they have no known competing financial interests or personal relationships that could have appeared to influence the work reported in this paper.

Appendix A. Supplementary data

Supplementary data to this article can be found online at https://doi.org/10.1016/j.heliyon.2023.e16598.

References

[1] E. Ozbay, Plasmonics: merging photonics and electronics at nanoscale dimensions, Science 311 (2006) 189–193.
[2] J.A. Schuller, E.S. Barnard, W. Cai, Y.C. Jun, J.S. White, M.L. Brongersma, Plasmonics for extreme light concentration and manipulation, Nat. Mater. 9 (2010) 193–204.
[3] D.K. Gramotnev, S.I. Bozhevolnyi, Plasmonics beyond the diffraction limit, Nat. Photonics 4 (2010) 83–91.
[4] Z. Fang, X. Zhu, Plasmonics in nanostructures, Adv. Mater. 25 (2013) 3840–3856.
[5] A.G. Brolo, Plasmonics for future biosensors, Nat. Photonics 6 (2012) 709–713.
[6] J.R. Mejia-Salazar, O.N. Oliveira Jr., Plasmonic Biosensing. Chem. Rev. 118 (2018) 10617–10625.
[7] K. Yang, X. Yao, B. Liu, B. Ren, Metallic plasmonic array structures: principles, fabrications, properties, and applications, Adv. Mater. (2021), 2007988.
[8] C. Valsecchi, A.G. Brolo, Periodic metallic nanostructures as plasmonic chemical sensors, Langmuir 29 (2013) 5638–5649.
[9] N. Mudgal, A. Saharia, K.K. Choure, A. Agarwal, G. Singh, Sensitivity enhancement with anti-reflection coating of silicon nitride (Si3N4) layer in silver-based Surface Plasmon Resonance (SPR) sensor for sensing of DNA hybridization, Appl. Phys. A 126 (2020) 946.
[10] Y. Shen, J. Zhou, T. Liu, Y. Tao, R. Jiang, M. Liu, G. Xiao, J. Zhu, Z.K. Zhou, X. Wang, C. Jin, J. Wang, Plasmonic gold mushroom arrays with refractive index sensing figures of merit approaching the theoretical limit, Nat. Commun. 4 (2013) 2381.
[11] B. Liu, S. Chen, J. Zhang, X. Yao, J. Zhong, H. Lin, T. Huang, Z. Yang, J. Zhu, S. Liu, C. Lienau, L. Wang, B. Ren, A plasmonic sensor array with ultrahigh figures of merit and resonance linewidths down to 3 nm, Adv. Mater. 30 (2018), 1706031.
[12] W. Zhang, O.J.F. Martin, A universal law for plasmon resonance shift in biosensing, ACS Photonics 2 (2014) 144–150.
[13] J. Yang, H. Giessen, P. Lalanne, Simple analytical expression for the peak-frequency shifts of plasmonic resonances for sensing, Nano Lett. 15 (2015) 3439–3444.
[14] S.Y. Ding, E.M. You, Z.Q. Tian, M. Moskovits, Electromagnetic theories of surface-enhanced Raman spectroscopy, Chem. Soc. Rev. 46 (2017) 4042–4076.

[15] W. Chen, S. Zhang, Q. Deng, H. Xu, Probing of sub-picometer vertical differential resolutions using cavity plasmons, Nat. Commun. 9 (2018) 801.
[16] S. Link, M.A. El-Sayed, Shape and size dependence of radiative, non-radiative and photothermal properties of gold nanocrystals, Int. Rev. Phys. Chem. 19 (2000) 409–453.
[17] C. Sonnichsen, T. Franzl, T. Wilk, G. von Plessen, J. Feldmann, O. Wilson, P. Mulvaney, Drastic reduction of plasmon damping in gold nanorods, Phys. Rev. Lett. 88 (2002), 077402.
[18] K.M. Mayer, J.H. Hafner, Localized surface plasmon resonance sensors, Chem. Rev. 111 (2011) 3828–3857.
[19] K.A. Willets, R.P. Van Duyne, Localized surface plasmon resonance spectroscopy and sensing, Annu. Rev. Phys. Chem. 58 (2007) 267–297.
[20] E. Petryayeva, U.J. Krull, Localized surface plasmon resonance: nanostructures, bioassays and biosensing–a review, Anal. Chim. Acta 706 (2011) 8–24.
[21] A.A. Yanik, A.E. Cetin, M. Huang, A. Artar, S.H. Mousavi, A. Khanikaev, J.H. Connor, G. Shvets, H. Altug, Seeing protein monolayers with naked eye through plasmonic Fano resonances, Proc. Natl. Acad. Sci. USA 108 (2011) 11784–11789.
[22] Y. Liang, H. Zhang, W. Zhu, A. Agrawal, H. Lezec, L. Li, W. Peng, Y. Zou, Y. Lu, T. Xu, Subradiant dipolar interactions in plasmonic nanoring resonator array for integrated label-free biosensing, ACS Sens. 2 (2017) 1796–1804.
[23] Z. Shen, M. Du, High-performance refractive index sensing system based on multiple Fano resonances in polarization-insensitive metasurface with nanorings, Opt Express 29 (2021) 28287–28296.
[24] M. Bunruangses, P. Youplao, I. Sadegh Amiri, N. Pornsuwancharoen, S. Punthawanunt, G. Singh, P. Yupapin, Microring distributed sensors using space-time function control, IEEE Sensor. J. 20 (2020) 799–805.
[25] J.F. Masson, Surface plasmon resonance clinical biosensors for medical diagnostics, ACS Sens. 2 (2017) 16–30.
[26] S.N. Nangare, P.O. Patil, Affinity-based nanoarchitectured biotransducer for sensitivity enhancement of surface plasmon resonance sensors for in vitro diagnosis: a review, ACS Biomater. Sci. Eng. 7 (2021) 2–30.
[27] R. Zafar, S. Nawaz, G. Singh, A. d'Alessandro, M. Salim, Plasmonics-based refractive index sensor for detection of hemoglobin concentration, IEEE Sensor. J. 18 (2018) 4372–4377.
[28] J. Homola, Surface plasmon resonance sensors for detection of chemical and biological species, Chem. Rev. 108 (2008) 462–493.
[29] S. Rebe Raz, H. Liu, W. Norde, M.G. Bremer, Food allergens profiling with an imaging surface plasmon resonance-based biosensor, Anal. Chem. 82 (2010) 8485–8491.
[30] B.J. Yakes, J. Deeds, K. White, S.L. Degrasse, Evaluation of surface plasmon resonance biosensors for detection of tetrodotoxin in food matrices and comparison to analytical methods, J. Agric. Food Chem. 59 (2011) 839–846.
[31] J. Liu, M. Jalali, S. Mahshid, S. Wachsmann-Hogiu, Are plasmonic optical biosensors ready for use in point-of-need applications? Analyst 145 (2020) 364–384.
[32] J. Olson, S. Dominguez-Medina, A. Hoggard, L.Y. Wang, W.S. Chang, S. Link, Optical characterization of single plasmonic nanoparticles, Chem. Soc. Rev. 44 (2015) 40–57.
[33] G.V. Hartland, Optical studies of dynamics in noble metal nanostructures, Chem. Rev. 111 (2011) 3858–3887.
[34] A. Hoggard, L.Y. Wang, L. Ma, Y. Fang, G. You, J. Olson, Z. Liu, W.S. Chang, P.M. Ajayan, S. Link, Using the plasmon linewidth to calculate the time and efficiency of electron transfer between gold nanorods and graphene, ACS Nano 7 (2013) 11209–11217.
[35] P. Zijlstra, P.M. Paulo, K. Yu, Q.H. Xu, M. Orrit, Chemical interface damping in single gold nanorods and its near elimination by tip-specific functionalization, Angew. Chem. Int. Ed. 51 (2012) 8352–8355.
[36] C. Novo, D. Gomez, J. Perez-Juste, Z. Zhang, H. Petrova, M. Reismann, P. Mulvaney, G.V. Hartland, Contributions from radiation damping and surface scattering to the linewidth of the longitudinal plasmon band of gold nanorods: a single particle study, Phys. Chem. Chem. Phys. 8 (2006) 3540–3546.
[37] W.A. Kraus, G.C. Schatz, Plasmon resonance broadening in small metal particles, J. Chem. Phys. 79 (1983) 6130–6139.
[38] S.S.E. Collins, E.K. Searles, L.J. Tauzin, M. Lou, L. Bursi, Y. Liu, J. Song, C. Flatebo, R. Baiyasi, Y.Y. Cai, B. Foerster, T. Lian, P. Nordlander, S. Link, C.F. Landes, Plasmon energy transfer in hybrid nanoantennas, ACS Nano 15 (2021) 9522–9530.
[39] R.F. Oulton, Loss and gain, Nat. Photonics 6 (2012) 219–221.
[40] A. Konrad, F. Wackenhut, M. Hussels, A.J. Meixner, M. Brecht, Temperature dependent luminescence and dephasing of gold nanorods, J. Phys. Chem. C 117 (2013) 21476–21482.
[41] M. Liu, M. Pelton, P. Guyot-Sionnest, Reduced damping of surface plasmons at low temperatures, Phys. Rev. B 79 (2009), 035418.
[42] W. Jiang, H. Hu, Q. Deng, S. Zhang, H. Xu, Temperature-dependent dark-field scattering of single plasmonic nanocavity, Nanophotonics 9 (2020) 3347–3356.
[43] A. De Luca, M.P. Grzelczak, I. Pastoriza-Santos, L.M. Liz-Marzan, M. La Deda, M. Striccoli, G. Strangi, Dispersed and encapsulated gain medium in plasmonic nanoparticles: a multipronged approach to mitigate optical losses, ACS Nano 5 (2011) 5823–5829.
[44] L. Meng, D. Zhao, Y. Yang, F.J. García de Abajo, Q. Li, Z. Ruan, M. Qiu, Gain-assisted plasmon resonance narrowing and its application in sensing, Phys. Rev. Appl. 11 (2019), 044030.
[45] A. De Luca, M. Ferrie, S. Ravaine, M. La Deda, M. Infusino, A.R. Rashed, A. Veltri, A. Aradian, N. Scaramuzza, G. Strangi, Gain functionalized core–shell nanoparticles: the way to selectively compensate absorptive losses, J. Mater. Chem. 22 (2012) 8846–8852.
[46] V.G. Kravets, A.V. Kabashin, W.L. Barnes, A.N. Grigorenko, Plasmonic surface lattice resonances: a review of properties and applications, Chem. Rev. 118 (2018) 5912–5951.
[47] L. Lin, Y. Zheng, Engineering of parallel plasmonic-photonic interactions for on-chip refractive index sensors, Nanoscale 7 (2015) 12205–12214.
[48] A. Danilov, G. Tselikov, F. Wu, V.G. Kravets, I. Ozerov, F. Bedu, A.N. Grigorenko, A.V. Kabashin, Ultra-narrow surface lattice resonances in plasmonic metamaterial arrays for biosensing applications, Biosens. Bioelectron. 104 (2018) 102–112.
[49] R.R. Gutha, S.M. Sadeghi, C. Sharp, W.J. Wing, Biological sensing using hybridization phase of plasmonic resonances with photonic lattice modes in arrays of gold nanoantennas, Nanotechnology 28 (2017), 355504.
[50] S. Zou, N. Janel, G.C. Schatz, Silver nanoparticle array structures that produce remarkably narrow plasmon lineshapes, J. Chem. Phys. 120 (2004) 10871–10875.
[51] S. Zou, G.C. Schatz, Narrow plasmonic/photonic extinction and scattering line shapes for one and two dimensional silver nanoparticle arrays, J. Chem. Phys. 121 (2004) 12606–12612.
[52] P. Offermans, M.C. Schaafsma, S.R. Rodriguez, Y. Zhang, M. Crego-Calama, S.H. Brongersma, J. Gomez Rivas, Universal scaling of the figure of merit of plasmonic sensors, ACS Nano 5 (2011) 5151–5157.
[53] A.D. Humphrey, W.L. Barnes, Plasmonic surface lattice resonances on arrays of different lattice symmetry, Phys. Rev. B 90 (2014), 075404.
[54] B. Luk'yanchuk, N.I. Zheludev, S.A. Maier, N.J. Halas, P. Nordlander, H. Giessen, C.T. Chong, The Fano resonance in plasmonic nanostructures and metamaterials, Nat. Mater. 9 (2010) 707–715.
[55] M. Rahmani, B. Luk'yanchuk, M. Hong, Fano resonance in novel plasmonic nanostructures, Laser Photon. Rev. 7 (2013) 329–349.
[56] M.F. Limonov, M.V. Rybin, A.N. Poddubny, Y.S. Kivshar, Fano resonances in photonics, Nat. Photonics 11 (2017) 543–554.
[57] A.E. Miroshnichenko, S. Flach, Y.S. Kivshar, Fano resonances in nanoscale structures, Rev. Mod. Phys. 82 (2010) 2257–2298.
[58] A. Lotfiani, S.M. Mohseni, M. Ghanaatshoar, High-sensitive optoelectronic SPR biosensor based on Fano resonance in the integrated MIM junction and optical layers, Opt Commun. 477 (2020), 126323.
[59] M.A. Butt, N.L. Kazanskiy, S.N. Khonina, Nanodots decorated asymmetric metal–insulator–metal waveguide resonator structure based on Fano resonances for refractive index sensing application, Laser Phys. 30 (2020), 076204.
[60] S. Zhang, G.-C. Li, Y. Chen, X. Zhu, S.-D. Liu, D.Y. Lei, H. Duan, Pronounced fano resonance in single gold split nanodisks with 15 nm split gaps for intensive second harmonic generation, ACS Nano 10 (2016) 11105–11114.
[61] Z. Fang, J. Cai, Z. Yan, P. Nordlander, N.J. Halas, X. Zhu, Removing a wedge from a metallic nanodisk reveals a fano resonance, Nano Lett. 11 (2011) 4475–4479.
[62] D.-J. Cai, Y.-H. Huang, W.-J. Wang, W.-B. Ji, J.-D. Chen, Z.-H. Chen, S.-D. Liu, Fano resonances generated in a single dielectric homogeneous nanoparticle with high structural symmetry, J. Phys. Chem. C 119 (2015) 4252–4260.

[63] W. Wan, W. Zheng, Y. Chen, Z. Liu, From Fano-like interference to superscattering with a single metallic nanodisk, Nanoscale 6 (2014) 9093–9102.
[64] G. Bachelier, I. Russier-Antoine, E. Benichou, C. Jonin, N. Del Fatti, F. Vallee, P.F. Brevet, Fano profiles induced by near-field coupling in heterogeneous dimers of gold and silver nanoparticles, Phys. Rev. Lett. 101 (2008), 197401.
[65] O. Peña-Rodríguez, U. Pal, M. Campoy-Quiles, L. Rodríguez-Fernández, M. Garriga, M.I. Alonso, Enhanced fano resonance in asymmetrical Au:Ag heterodimers, J. Phys. Chem. C 115 (2011) 6410–6414.
[66] A.E. Cetin, H. Altug, Fano resonant ring/disk plasmonic nanocavities on conducting substrates for advanced biosensing, ACS Nano 6 (2012) 9989–9995.
[67] J. Ye, F. Wen, H. Sobhani, J.B. Lassiter, P. Van Dorpe, P. Nordlander, N.J. Halas, Plasmonic nanoclusters: near field properties of the Fano resonance interrogated with SERS, Nano Lett. 12 (2012) 1660–1667.
[68] M. Hentschel, M. Saliba, R. Vogelgesang, H. Giessen, A.P. Alivisatos, N. Liu, Transition from isolated to collective modes in plasmonic oligomers, Nano Lett. 10 (2010) 2721–2726.
[69] N.S. King, L. Liu, X. Yang, B. Cerjan, H.O. Everitt, P. Nordlander, N.J. Halas, Fano resonant aluminum nanoclusters for plasmonic colorimetric sensing, ACS Nano 9 (2015) 10628–10636.
[70] M.A. Butt, S.N. Khonina, N.L. Kazanskiy, Simple and improved plasmonic sensor configuration established on MIM waveguide for enhanced sensing performance, Plasmonics 17 (2022) 1305–1314.
[71] M.A. Schmidt, D.Y. Lei, L. Wondraczek, V. Nazabal, S.A. Maier, Hybrid nanoparticle-microcavity-based plasmonic nanosensors with improved detection resolution and extended remote-sensing ability, Nat. Commun. 3 (2012) 1108.
[72] Z. Liu, J. Ye, Highly controllable double Fano resonances in plasmonic metasurfaces, Nanoscale 8 (2016) 17665–17674.
[73] D. Chanda, K. Shigeta, T. Truong, E. Lui, A. Mihi, M. Schulmerich, P.V. Braun, R. Bhargava, J.A. Rogers, Coupling of plasmonic and optical cavity modes in quasi-three-dimensional plasmonic crystals, Nat. Commun. 2 (2011) 479.
[74] R. Ameling, L. Langguth, M. Hentschel, M. Mesch, P.V. Braun, H. Giessen, Cavity-enhanced localized plasmon resonance sensing, Appl. Phys. Lett. 97 (2010), 253116.
[75] R. Ameling, H. Giessen, Microcavity plasmonics: strong coupling of photonic cavities and plasmons, Laser Photon. Rev. 7 (2013) 141–169.
[76] W. Zhu, T. Xu, H. Wang, C. Zhang, P.B. Deotare, A. Agrawal, H.J. Lezec, Surface plasmon polariton laser based on a metallic trench Fabry-Perot resonator, Sci. Adv. 3 (2017), e1700909.
[77] Y.-L. Ho, A. Portela, Y. Lee, E. Maeda, H. Tabata, J.-J. Delaunay, Hollow plasmonic U-cavities with high-aspect-ratio nanofins sustaining strong optical vortices for light trapping and sensing, Adv. Opt. Mater. 2 (2014) 522–528.
[78] M.W. Knight, Y. Wu, J.B. Lassiter, P. Nordlander, N. Halas, J. Substrates matter: influence of an adjacent dielectric on an individual plasmonic nanoparticle, Nano Lett. 9 (2009) 2188–2192.
[79] L.J. Sherry, S.H. Chang, G.C. Schatz, R.P. Van Duyne, B.J. Wiley, Y. Xia, Localized surface plasmon resonance spectroscopy of single silver nanocubes, Nano Lett. 5 (2005) 2034–2038.
[80] A. Sobhani, A. Manjavacas, Y. Cao, M.J. McClain, F.J. Garcia de Abajo, P. Nordlander, N.J. Halas, Pronounced linewidth narrowing of an aluminum nanoparticle plasmon resonance by interaction with an aluminum metallic film, Nano Lett. 15 (2015) 6946–6951.
[81] G.C. Li, Y.L. Zhang, J. Jiang, Y. Luo, D.Y. Lei, Metal-substrate-mediated plasmon hybridization in a nanoparticle dimer for photoluminescence line-width shrinking and intensity enhancement, ACS Nano 11 (2017) 3067–3080.
[82] M. Kaliteevski, I. Iorsh, S. Brand, R.A. Abram, J.M. Chamberlain, A.V. Kavokin, I.A. Shelykh, Tamm plasmon-polaritons: possible electromagnetic states at the interface of a metal and a dielectric Bragg mirror, Phys. Rev. B 76 (2007), 165415.
[83] H. Lu, Y. Li, H. Jiao, Z. Li, D. Mao, J. Zhao, Induced reflection in Tamm plasmon systems, Opt Express 27 (2019) 5383–5392.
[84] Z. Wang, Y.L. Ho, T. Cao, T. Yatsui, J.J. Delaunay, High-Q and tailorable fano resonances in a one-dimensional metal-optical Tamm state structure: from a narrowband perfect absorber to a narrowband perfect reflector, Adv. Funct. Mater. 31 (2021), 2102183.
[85] B. Wang, P. Yu, W. Wang, X. Zhang, H.C. Kuo, H. Xu, Z.M. Wang, High-Q plasmonic resonances: fundamentals and applications, Adv. Opt. Mater. 9 (2021), 2001520.
[86] A. Kumari, S. Kumar, M.K. Shukla, G. Kumar, P.S. Maji, R. Vijaya, R. Das, Coupling to Tamm-plasmon-polaritons: dependence on structural parameters, J. Phys. D Appl. Phys. 51 (2018), 255103.
[87] W. Chen, S. Kaya Ozdemir, G. Zhao, J. Wiersig, L. Yang, Exceptional points enhance sensing in an optical microcavity, Nature 548 (2017) 192–196.
[88] X. Jiang, L. Shao, S.X. Zhang, X. Yi, J. Wiersig, L. Wang, Q. Gong, M. Loncar, L. Yang, Y.F. Xiao, Chaos-assisted broadband momentum transformation in optical microresonators, Science 358 (2017) 344–347.
[89] N. Toropov, G. Cabello, M.P. Serrano, R.R. Gutha, M. Rafti, F. Vollmer, Review of biosensing with whispering-gallery mode lasers, Light Sci. Appl. 10 (2021) 42.
[90] Q. Ai, L. Gui, D. Paone, B. Metzger, M. Mayer, K. Weber, A. Fery, H. Giessen, Ultranarrow second-harmonic resonances in hybrid plasmon-fiber cavities, Nano Lett. 18 (2018) 5576–5582.
[91] F. Pan, K.C. Smith, H.L. Nguyen, K.A. Knapper, D.J. Masiello, R.H. Goldsmith, Elucidating energy pathways through simultaneous measurement of absorption and transmission in a coupled plasmonic-photonic cavity, Nano Lett. 20 (2020) 50–58.
[92] Y. Chen, Y. Yin, L. Ma, O.G. Schmidt, Recent progress on optoplasmonic whispering gallery mode microcavities, Adv. Opt. Mater. 9 (2021).
[93] P. Wang, Y. Wang, Z. Yang, X. Guo, X. Lin, X.C. Yu, Y.F. Xiao, W. Fang, L. Zhang, G. Lu, Q. Gong, L. Tong, Single-Band 2-nm-Line-Width plasmon resonance in a strongly coupled Au nanorod, Nano Lett. 15 (2015) 7581–7586.
[94] K.V. Sreekanth, Y. Alapan, M. ElKabbash, E. Ilker, M. Hinczewski, U.A. Gurkan, A. De Luca, G. Strangi, Extreme sensitivity biosensing platform based on hyperbolic metamaterials, Nat. Mater. 15 (2016) 621–627.
[95] Y.D. Jin, Engineering plasmonic gold nanostructures and metamaterials for biosensing and nanomedicine, Adv. Mater. 24 (2012) 5153–5165.
[96] M.S. Luchansky, R.C. Bailey, High-Q optical sensors for chemical and biological analysis, Anal. Chem. 84 (2012) 793–821.
[97] J.Q. Li, C. Chen, L. Lagae, P. Van Dorpe, Nanoplasmonic sensors with various photonic coupling effects for detecting different targets, J. Phys. Chem. C 119 (2015) 29116–29122.
[98] R. Daniel, T. Andreas, A.B. Nadine, J.H. Aurelian, L. Odeta, K. Christopher, Y. Daehan, N.J. Wittenberg, O. Sang-Hyun, H.A. Lashuel, Resolving molecule-specific information in dynamic lipid membrane processes with multi-resonant infrared metasurfaces, Nat. Commun. 9 (2018) 2160.
[99] C. Zhan, B.W. Liu, Z.Q. Tian, B. Ren, Determining the interfacial refractive index via ultrasensitive plasmonic sensors, J. Am. Chem. Soc. 142 (2020) 10905–10909.
[100] H. Im, H. Shao, Y.I. Park, V.M. Peterson, C.M. Castro, R. Weissleder, H. Lee, Label-free detection and molecular profiling of exosomes with a nano-plasmonic sensor, Nat. Biotechnol. 32 (2014) 490–495.
[101] A.E. Cetin, D. Etezadi, B.C. Galarreta, M.P. Busson, Y. Eksioglu, H. Altug, Plasmonic nanohole arrays on a robust hybrid substrate for highly sensitive label-free biosensing, ACS Photonics 2 (2015) 1167–1174.
[102] L.K. Chin, T. Son, J.S. Hong, A.Q. Liu, J. Skog, C.M. Castro, R. Weissleder, H. Lee, H. Im, Plasmonic sensors for extracellular vesicle analysis: from scientific development to translational research, ACS Nano 14 (2020) 14528–14548.
[103] C. Liu, X. Zeng, Z. An, Y. Yang, M. Eisenbaum, X. Gu, J.M. Jornet, G.K. Dy, M.E. Reid, Q. Gan, Y. Wu, Sensitive detection of exosomal proteins via a compact surface plasmon resonance biosensor for cancer diagnosis, ACS Sens. 3 (2018) 1471–1479.
[104] A. Rezabakhsh, R. Rahbarghazi, F. Fathi, Surface plasmon resonance biosensors for detection of Alzheimer's biomarkers; an effective step in early and accurate diagnosis, Biosens. Bioelectron. 167 (2020), 112511.
[105] S. Mittal, A. Saharia, Y. Ismail, F. Petruccione, A.V. Bourdine, O.G. Morozov, V.V. Demidov, J. Yin, G. Singh, M. Tiwari, Spiral shaped photonic crystal fiber-based surface plasmon resonance biosensor for cancer cell detection, Photonics 10 (2023) 230.
[106] N. Fabri-Faja, O. Calvo-Lozano, P. Dey, R.A. Terborg, M.C. Estevez, A. Belushkin, F. Yesilkoy, L. Duempelmann, H. Altug, V. Pruneri, L.M. Lechuga, Early sepsis diagnosis via protein and miRNA biomarkers using a novel point-of-care photonic biosensor, Anal. Chim. Acta 1077 (2019) 232–242.

[107] G.K. Joshi, S. Deitz-McElyea, M. Johnson, S. Mali, M. Korc, R. Sardar, Highly specific plasmonic biosensors for ultrasensitive microRNA detection in plasma from pancreatic cancer patients, Nano Lett. 14 (2014) 6955–6963.
[108] G.K. Joshi, S. Deitz-McElyea, T. Liyanage, K. Lawrence, S. Mali, R. Sardar, M. Korc, Label-free nanoplasmonic-based short noncoding RNA sensing at attomolar concentrations allows for quantitative and highly specific assay of MicroRNA-10b in biological fluids and circulating exosomes, ACS Nano 9 (2015) 11075–11089.
[109] X. Li, M. Soler, C.I. Ozdemir, A. Belushkin, F. Yesilkoy, H. Altug, Plasmonic nanohole array biosensor for label-free and real-time analysis of live cell secretion, Lab Chip 17 (2017) 2208–2217.
[110] S.-K. Lee, B. Yim, J. Park, N.-G. Kim, B.-S. Kim, Y. Park, Y.K. Yoon, J. Kim, Method for the rapid detection of SARS-CoV-2-neutralizing antibodies using a nanogel-based surface plasmon resonance biosensor, ACS Appl. Polym. Mater. 5 (2023) 2195–2202.
[111] F. Li, J. Hong, C. Guan, K. Chen, Y. Xie, Q. Wu, J. Chen, B. Deng, J. Shen, X. Liu, R. Hu, Y. Zhang, Y. Chen, J. Zhu, Affinity exploration of SARS-CoV-2 RBD variants to mAb-functionalized plasmonic metasurfaces for label-free immunoassay boosting, ACS Nano 17 (2023) 3383–3393.
[112] J. Gomez-Cruz, S. Nair, A. Manjarrez-Hernandez, S. Gavilanes-Parra, G. Ascanio, C. Escobedo, Cost-effective flow-through nanohole array-based biosensing platform for the label-free detection of uropathogenic E. coli in real time, Biosens. Bioelectron. 106 (2018) 105–110.
[113] A. Prasad, J. Choi, Z. Jia, S. Park, M.R. Gartia, Nanohole array plasmonic biosensors: emerging point-of-care applications, Biosens. Bioelectron. 130 (2019) 185–203.
[114] J. Zhou, Q. Qi, C. Wang, Y. Qian, G. Liu, Y. Wang, L. Fu, Surface plasmon resonance (SPR) biosensors for food allergen detection in food matrices, Biosens. Bioelectron. 142 (2019), 111449.
[115] D.D. Galvan, V. Parekh, E. Liu, E.L. Liu, Q. Yu, Sensitive bacterial detection via dielectrophoretic-enhanced mass transport using surface-plasmon-resonance biosensors, Anal. Chem. 90 (2018) 14635–14642.
[116] F. Melaine, M. Saad, S. Faucher, M. Tabrizian, Selective and high dynamic range assay format for multiplex detection of pathogenic Pseudomonas aeruginosa, Salmonella typhimurium, and Legionella pneumophila RNAs using surface plasmon resonance imaging, Anal. Chem. 89 (2017) 7802–7807.
[117] A.N. Masterson, B.B. Muhoberac, A. Gopinadhan, D.J. Wilde, F.T. Deiss, C.C. John, R. Sardar, Multiplexed and high-throughput label-free detection of RNA/spike protein/IgG/IgM biomarkers of SARS-CoV-2 infection utilizing nanoplasmonic biosensors, Anal. Chem. 93 (2021) 8754–8763.
[118] I. Zoric, E.M. Larsson, B. Kasemo, C. Langhammer, Localized surface plasmons shed light on nanoscale metal hydrides, Adv. Mater. 22 (2010) 4628–4633.
[119] N. Liu, M.L. Tang, M. Hentschel, H. Giessen, A.P. Alivisatos, Nanoantenna-enhanced gas sensing in a single tailored nanofocus, Nat. Mater. 10 (2011) 631–636.
[120] C. Wadell, S. Syrenova, C. Langhammer, Plasmonic hydrogen sensing with nanostructured metal hydrides, ACS Nano 8 (2014) 11925–11940.
[121] H. Huang, S. Chen, F. Liu, Q. Zhao, B. Liao, S. Yi, Y. Zeng, Multiplex plasmonic sensor for detection of different metal ions based on a single type of gold nanorod, Anal. Chem. 85 (2013) 2312–2319.
[122] L. Ding, Y. Gao, J. Di, A sensitive plasmonic copper(II) sensor based on gold nanoparticles deposited on ITO glass substrate, Biosens. Bioelectron. 83 (2016) 9–14.
[123] Y. Zhao, K. Mukherjee, K.D. Benkstein, L. Sun, K.L. Steffens, C.B. Montgomery, S. Guo, S. Semancik, M.E. Zaghloul, Miniaturized nanohole array based plasmonic sensor for the detection of acetone and ethanol with insights into the kinetics of adsorptive plasmonic sensing, Nanoscale 11 (2019) 11922–11932.
[124] Y. Shen, X. She, C. Jin, Mechanically reconfigurable Pd nanogroove array: an ultrasensitive optical hydrogen detector, ACS Photonics 5 (2018) 1334–1342.
[125] A.A. Yanik, M. Huang, O. Kamohara, A. Artar, T.W. Geisbert, J.H. Connor, H. Altug, An optofluidic nanoplasmonic biosensor for direct detection of live viruses from biological media, Nano Lett. 10 (2010) 4962–4969.
[126] K. Lee, K. Fraser, B. Ghaddar, K. Yang, E. Kim, L. Balaj, E.A. Chiocca, X.O. Breakefield, H. Lee, R. Weissleder, Multiplexed profiling of single extracellular vesicles, ACS Nano 12 (2018) 494–503.
[127] I. Darmadi, S.Z. Khairunnisa, D. Tomeček, C. Langhammer, Optimization of the composition of PdAuCu ternary alloy nanoparticles for plasmonic hydrogen sensing, ACS Appl. Nano Mater. 4 (2021) 8716–8722.
[128] J.H. Qu, K. Leirs, W. Maes, M. Imbrechts, N. Callewaert, K. Lagrou, N. Geukens, J. Lammertyn, D. Spasic, Innovative FO-SPR label-free strategy for detecting anti-RBD antibodies in COVID-19 patient serum and whole blood, ACS Sens. 7 (2022) 477–487.
[129] H. Zhu, Y. Lu, J. Xia, Y. Liu, J. Chen, J. Lee, K. Koh, H. Chen, Aptamer-assisted protein orientation on silver magnetic nanoparticles: application to sensitive leukocyte cell-derived chemotaxin 2 surface plasmon resonance sensors, Anal. Chem. 94 (2022) 2109–2118.
[130] I. Malkiel, M. Mrejen, A. Nagler, U. Arieli, L. Wolf, H. Suchowski, Plasmonic nanostructure design and characterization via Deep Learning, Light Sci. Appl. 7 (2018) 60.
[131] J. Smajic, C. Hafner, L. Raguin, K. Tavzarashvili, M. Mishrikey, Comparison of numerical methods for the analysis of plasmonic structures, J. Comput. Theor. Nanosci. 6 (2009) 763–774.
[132] A.F. Oskooi, D. Roundy, M. Ibanescu, P. Bermel, J.D. Joannopoulos, S.G. Johnson, MEEP: a flexible free-software package for electromagnetic simulations by the FDTD method, Comput. Phys. Commun. 181 (2010) 687–702.
[133] M.A. Bessa, P. Glowacki, M. Houlder, Bayesian machine learning in metamaterial design: fragile becomes supercompressible, Adv. Mater. 31 (2019), 1904845.
[134] Z. Huang, X. Liu, J. Zang, The inverse design of structural color using machine learning, Nanoscale 11 (2019) 21748–21758.
[135] W. Ma, F. Cheng, Y. Xu, Q. Wen, Y. Liu, Probabilistic representation and inverse design of metamaterials based on a deep generative model with semi-supervised learning strategy, Adv. Mater. 31 (2019), 1901111.
[136] J. Zhou, B. Huang, Z. Yan, J.G. Bunzli, Emerging role of machine learning in light-matter interaction, Light Sci. Appl. 8 (2019) 84.
[137] A.P. Blanchard-Dionne, O.J.F. Martin, Teaching optics to a machine learning network, Opt. Lett. 45 (2020) 2922–2925.
[138] P.R. Wiecha, O.L. Muskens, Deep learning meets nanophotonics: a generalized accurate predictor for near fields and far fields of arbitrary 3D nanostructures, Nano Lett. 20 (2020) 329–338.
[139] F. Cui, Y. Yue, Y. Zhang, Z. Zhang, H.S. Zhou, Advancing biosensors with machine learning, ACS Sens. 5 (2020) 3346–3364.
[140] A. Tittl, A. John-Herpin, A. Leitis, E.R. Arvelo, H. Altug, Metasurface-based molecular biosensing aided by artificial intelligence, Angew. Chem. Int. Ed. 58 (2019) 14810–14822.
[141] A. Boltasseva, H.A. Atwater, Materials science. Low-loss plasmonic metamaterials, Science 331 (2011) 290–291.
[142] G.V. Naik, V.M. Shalaev, A. Boltasseva, Alternative plasmonic materials: beyond gold and silver, Adv. Mater. 25 (2013) 3264–3294.
[143] J.B. Khurgin, How to deal with the loss in plasmonics and metamaterials, Nat. Nanotechnol. 10 (2015) 2–6.
[144] Y. Wang, J. Yu, Y.F. Mao, J. Chen, S. Wang, H.Z. Chen, Y. Zhang, S.Y. Wang, X. Chen, T. Li, L. Zhou, R.M. Ma, S. Zhu, W. Cai, J. Zhu, Stable, high-performance sodium-based plasmonic devices in the near infrared, Nature 581 (2020) 401–405.
[145] S.I. Azzam, V.M. Shalaev, A. Boltasseva, A.V. Kildishev, Formation of bound states in the continuum in hybrid plasmonic-photonic systems, Phys. Rev. Lett. 121 (2018), 253901.
[146] S. Romano, G. Zito, S. Torino, G. Calafiore, E. Penzo, G. Coppola, S. Cabrini, I. Rendina, V. Mocella, Label-free sensing of ultralow-weight molecules with all-dielectric metasurfaces supporting bound states in the continuum, Photon. Res. 6 (2018) 726–733.
[147] S.I. Azzam, A.V. Kildishev, Photonic bound states in the continuum: from basics to applications, Adv. Opt. Mater. 9 (2020), 2001469.
[148] C.W. Hsu, B. Zhen, J. Lee, S.L. Chua, S.G. Johnson, J.D. Joannopoulos, M. Soljacic, Observation of trapped light within the radiation continuum, Nature 499 (2013) 188–191.
[149] C.-L. Zou, J.-M. Cui, F.-W. Sun, X. Xiong, X.-B. Zou, Z.-F. Han, G.-C. Guo, Guiding light through optical bound states in the continuum for ultrahigh-Qmicroresonators, Laser Photon. Rev. 9 (2015) 114–119.
[150] C.W. Hsu, B. Zhen, A.D. Stone, J.D. Joannopoulos, M. Soljačić, Bound states in the continuum, Nat. Rev. Mater. 1 (2016), 16048.
[151] M. Meudt, C. Bogiadzi, K. Wrobel, P. Görrn, Hybrid photonic–plasmonic bound states in continuum for enhanced light manipulation, Adv. Opt. Mater. 8 (2020), 2000898.
[152] T. Xu, Z. Geng, Strategies to improve performances of LSPR biosensing: structure, materials, and interface modification, Biosens. Bioelectron. 174 (2021), 112850.

[153] A. Rana, Y. Zhang, L. Esfandiari, Advancements in microfluidic technologies for isolation and early detection of circulating cancer-related biomarkers, Analyst 143 (2018) 2971–2991.
[154] J. Sun, Y. Xianyu, X. Jiang, Point-of-care biochemical assays using gold nanoparticle-implemented microfluidics, Chem. Soc. Rev. 43 (2014) 6239–6253.
[155] O. Yavas, S.S. Acimovic, J. Garcia-Guirado, J. Berthelot, P. Dobosz, V. Sanz, R. Quidant, Self-calibrating on-chip localized surface plasmon resonance sensing for quantitative and multiplexed detection of cancer markers in human serum, ACS Sens. 3 (2018) 1376–1384.
[156] H. Sugai, S. Tomita, S. Ishihara, K. Yoshioka, R. Kurita, Microfluidic sensing system with a multichannel surface plasmon resonance chip: damage-free characterization of cells by pattern recognition, Anal. Chem. 92 (2020) 14939–14946.
[157] J. Tu, R.M. Torrente-Rodríguez, M. Wang, W. Gao, The Era of digital health: a review of portable and wearable affinity biosensors, Adv. Funct. Mater. 30 (2019), 1906713.
[158] J.F. Masson, Portable and field-deployed surface plasmon resonance and plasmonic sensors, Analyst 145 (2020) 3776–3800.
[159] M. Sharafeldin, J.J. Davis, Point of care sensors for infectious pathogens, Anal. Chem. 93 (2021) 184–197.
[160] P. Preechaburana, M.C. Gonzalez, A. Suska, D. Filippini, Surface plasmon resonance chemical sensing on cell phones, Angew. Chem. Int. Ed. 51 (2012) 11585–11588.
[161] L. Lu, Z. Jiang, Y. Hu, H. Zhou, G. Liu, Y. Chen, Y. Luo, Z. Chen, A portable optical fiber SPR temperature sensor based on a smart-phone, Opt Express 27 (2019) 25420–25427.
[162] Y. Liu, Q. Liu, S. Chen, F. Cheng, H. Wang, W. Peng, Surface plasmon resonance biosensor based on smart phone platforms, Sci. Rep. 5 (2015), 12864.
[163] M. Hentschel, M. Schaferling, X. Duan, H. Giessen, N. Liu, Chiral plasmonics, Sci. Adv. 3 (2017), e1602735.
[164] M. Matuschek, D.P. Singh, H.H. Jeong, M. Nesterov, T. Weiss, P. Fischer, F. Neubrech, N. Liu, Chiral plasmonic hydrogen sensors, Small 14 (2018), 1702990.
[165] W. Ma, L. Xu, L. Wang, C. Xu, H. Kuang, Chirality-based biosensors, Adv. Funct. Mater. 29 (2019), 1805512.
[166] F. Neubrech, M. Hentschel, N. Liu, Reconfigurable plasmonic chirality: fundamentals and applications, Adv. Mater. 32 (2020), 1905640.
[167] Y.Y. Lee, R.M. Kim, S.W. Im, M. Balamurugan, K.T. Nam, Plasmonic metamaterials for chiral sensing applications, Nanoscale 12 (2020) 58–66.
[168] X. Mu, L. Hu, Y. Cheng, Y. Fang, M. Sun, Chiral surface plasmon-enhanced chiral spectroscopy: principles and applications, Nanoscale 13 (2021) 581–601.
[169] G. Zheng, J. He, V. Kumar, S. Wang, I. Pastoriza-Santos, J. Perez-Juste, L.M. Liz-Marzan, K.Y. Wong, Discrete metal nanoparticles with plasmonic chirality, Chem. Soc. Rev. 50 (2021) 3738–3754.